

## Change in Crystal Structure of $\text{LiNi}_{0.8}\text{Co}_{0.19}\text{Cu}_{0.01}\text{O}_2$ Cathode during Charge of Coin Cell Observed by Ex Situ Time-of-flight Neutron Diffraction

Yasushi Idemoto,\*<sup>1</sup> Yuta Tsukada,<sup>1</sup> Naoto Kitamura,<sup>1</sup> Akinori Hoshikawa,<sup>2</sup> and Toru Ishigaki<sup>2</sup>

<sup>1</sup>Department of Pure and Applied Chemistry, Faculty of Science and Technology, Tokyo University of Science, 2641 Yamazaki, Noda, Chiba 278-8510

<sup>2</sup>Frontier Research Center for Applied Atomic Sciences, Ibaraki University, 162-1 Shirakawa, Tokai-mura, Naka-gun, Ibaraki 319-1106

(Received November 12, 2010; CL-100950; E-mail: idemoto@rs.noda.tus.ac.jp)

In the present study, we performed a new ex situ analysis of the change in the crystal structure of a cathode containing the composite material in a coin cell during the charge–discharge cycle. Time-of-flight neutron powder diffraction with Rietveld refinement was used to analyze the crystal structure of  $\text{LiNi}_{0.8}\text{Co}_{0.19}\text{Cu}_{0.01}\text{O}_2$  produced by solid-phase synthesis, both for the powder and a cathode before and after charging. The powder and the cathode had similar crystal structure parameters before charging. The results obtained demonstrate that crystal structure analysis by neutron diffraction is possible for a cathode containing 8.5 mg of active material. The results also showed that it is possible to quantitatively determine the Li composition, Li/Ni cation mixing amount, (Ni,Co,Cu)– $\text{O}_6$  octahedral distortion, and small quantities of the second phase component in the cathode before and after charging.

$\text{LiCoO}_2$  is currently used in the cathodes of most commercially available lithium-ion batteries. However, a great deal of research has been devoted to finding a substitute for cobalt, which is both expensive and toxic.<sup>1</sup> In our research, we have focused on a  $\text{Li}(\text{Ni},\text{Co})\text{O}_2$  system in which Co is substituted by Ni in  $\text{LiNiO}_2$ . With its relatively high capacitance and low Co content, this system is a promising replacement for  $\text{LiCoO}_2$ . However, Li is volatile at high temperatures and Li loss and cation mixing tend to occur under calcination. This is because  $\text{Ni}^{2+}$  has a similar radius (0.69 Å) to  $\text{Li}^+$  (0.76 Å) and it thus tends to occupy the empty site, resulting in inferior battery performance.<sup>2</sup> To resolve this problem, we synthesized a test material in which a portion of the (Ni, Co) is replaced by low-valence Cu with the aim of reducing the  $\text{Ni}^{2+}$  content to reduce cation mixing and thereby enhance the battery characteristics. To determine the amount of Li/Ni cation mixing, we have performed average structure analysis by neutron diffraction with Rietveld refinement.<sup>3</sup> This analysis has mainly been performed on the powder form that has not been subjected to charge–discharge cycling, but to determine the battery characteristics it is essential to determine changes in the crystal structure during the cycle. However, as the electrodes in coin cells contain relatively small amounts of active material, it has not been possible to perform structure analysis by neutron diffraction of samples subjected to charge–discharge.

In the present study, we performed ex situ measurements of the change in the crystal structure of the cathode material subjected to a charge–discharge cycle in a coin cell fabricated for this purpose. The results of time-of-flight neutron diffraction analysis of the cathode, which is composed of solid-phase-synthesized  $\text{LiNi}_{0.8}\text{Co}_{0.19}\text{Cu}_{0.01}\text{O}_2$  as the active cathode material

together with a conductor and a binder, before and after charging demonstrate that it is possible to determine the change in the crystal structure in an actual cathode containing 8.5 mg of active material.

$\text{LiNi}_{0.8}\text{Co}_{0.19}\text{Cu}_{0.01}\text{O}_2$  was synthesized by a solid-state method. To  $\text{LiOH}\cdot\text{H}_2\text{O}$  (purity: 98%, Wako Pure Chemical Industries, Ltd.),  $\text{Ni}(\text{OH})_2$  (purity: 98%, Wako Pure Chemical),  $\text{CoO}$  (purity: 98%, Wako Pure Chemical), and  $\text{CuO}$  (purity: 99.9%, Wako Pure Chemical), Ni was added in a fixed ratio of 3 mol % to precisely measured fixed ratios of Li, Co, and Cu. This mixture was dry blended for 1 h. The blend was then subjected to precalcination at 600 °C in air for 15 h and calcination at 800 °C in air for 15 h to obtain a powder sample.

The phase of the powder sample was analyzed by powder X-ray diffraction (Philips X'Pert Pro,  $\text{CuK}\alpha$  radiation) at a scanning rate of  $1^\circ \text{min}^{-1}$ , a tube voltage of 45 kV, a tube current of 40 mA, and a scanning range of  $2\theta = 10\text{--}70^\circ$ . The obtained diffraction patterns were then analyzed.

Compositional analysis of the metal content of the sample was performed using an inductively coupled plasma (ICP) emission spectrometer (ICPS-7500, ICPE-9000; Shimadzu Corp.).

The cell used for the charge–discharge experiments was a coin cell (HS cell; Hohsen Corp.). The cathode was fabricated by mixing acetylene black (AB) as the conductive material and poly(vinylidene difluoride) (PVdF) as the binder with the active material in the ratio active material:AB:PVdF = 85:10:5 (wt %). This mixture was then dispersed in *N*-methylpyrrolidone to form a slurry and applied to an Al foil (circular; diameter: 1 cm). It was dried and pressure bonded at approximately 40 MPa. The 1.5-cm-diameter circular anode was made from lithium, the electrolyte was a  $1 \text{ mol L}^{-1}$   $\text{LiPF}_6\text{--EC:DMC}$  (volume ratio; 1:2) solution (Kishida Chemical Co., Ltd.), and the separator was a polypropylene film. The cell was assembled in an argon-atmosphere glove box.

Charge–discharge experiments were performed using a charger–discharger (HJR-110m SM6; Hokuto Denko Corp.). The charge and discharge termination voltages were, 4.3 V vs.  $\text{Li/Li}^+$  and 2.5 V vs.  $\text{Li/Li}^+$  respectively, with charging and discharging at a constant current of  $0.2 \text{ mA cm}^{-2}$ . The circuit was held open for 2 min between charging and discharging. The cathode after charging was obtained in the second cycle at 30% Li separation (SOC 30%) after one charge–discharge cycle.

Neutron diffraction measurements were performed with a J-PARC iMATERIA (BL-20). The powder sample consisted of 0.8 g of active material and the measurement time was 55 min; the active-material content of the cathode prior to charging was approximately 8.5 mg and the measurement time was 188 min;

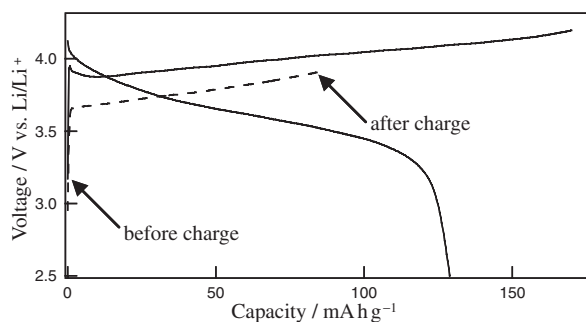


**Figure 1.** Charge–discharge curves of  $\text{LiNi}_{0.8}\text{Co}_{0.19}\text{Cu}_{0.01}\text{O}_2$  (temperature: 25 °C; current density: 0.2 mA cm<sup>-2</sup>; cut-off voltage: 2.5–4.3 V vs. Li/Li<sup>+</sup>). Solid lines: first cycle; dashed lines: second cycle.

the active-material content of the cathode after charging was approximately 8.5 mg and the measurement time was 383 min. The cathode measurement before charging was performed after stripping the Al foil current collector, whereas the cathode measurement after charging was performed without removing the Al foil. Crystal structure analysis was performed with Rietveld refinement using Z-Rietveld (ver. 0.9.34).<sup>4</sup>

The X-ray diffraction patterns of the  $\text{LiNi}_{0.8}\text{Co}_{0.19}\text{Cu}_{0.01}\text{O}_2$  powder clearly revealed (006)–(102) and (108)–(110) peak splitting, confirming the presence of a layered structure.<sup>5</sup> All peaks were assignable to an octahedral crystal (space group  $R\bar{3}m$ ), indicating that the powder consists of a single phase.

The compositions of the metal components were analyzed by ICP emission spectroscopy. When calculating the component ratios in the compositional formula, the total content of the powder sample was taken to be 2, and the total Ni, Co, and Cu contents in the electrode after charging were taken to be 1. The ratios were found to be Li:Ni:Co:Cu = 1.001(2):0.8042(1):0.1849(3):0.00980(2) for the powder sample and Li:Ni:Co:Cu = 0.613(3):0.804(1):0.1838(4):0.01171(5) for the electrode after charging.

Figure 1 shows the charge–discharge curves of the  $\text{LiNi}_{0.8}\text{Co}_{0.19}\text{Cu}_{0.01}\text{O}_2$ . The large irreversible capacity evident in this figure is attributable to the formation of a solid electrolyte interface layer in the first cycle.<sup>6</sup> The sample after charging was the second-cycle (SOC 30%) sample.

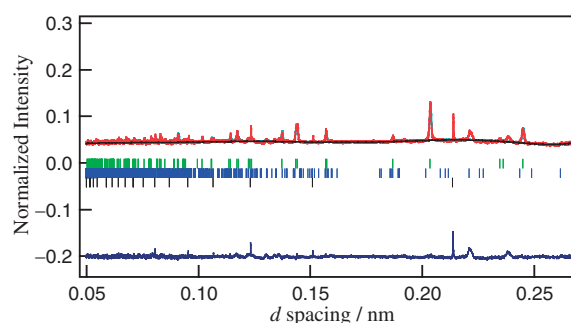
When investigating the crystal structure of the powder sample and the electrode before and after charging, analysis was performed for a hexagonal crystal (space group:  $R\bar{3}m$ ) with Li at the 3a site (0,0,0), the transition metal at the 3b site (0,0,1/2), and oxygen at the 6c site (0,0,*z*). The metal component occupancies were analyzed by employing the Li and Ni occupancy ratio as the variable for determining the cation mixing amount and by using the composition determined by ICP emission spectroscopy as a reference. The second phase could not be observed by X-ray diffraction; however, because the  $\text{Li}_2\text{CO}_3$  peak was observable in neutron diffraction, it was taken to be the second phase. For all the samples, there was close agreement between the measured and calculated values.

Table 1 shows the crystal structure parameters for the powder  $\text{LiNi}_{0.8}\text{Co}_{0.19}\text{Cu}_{0.01}\text{O}_2$ . Figure 2 shows the profile fitting results for the cathode of the coin cell prior to charging, and Table 2 shows its crystal structure parameters. The vessel vanadium (V) and the small quantity of  $\text{Li}_2\text{CO}_3$  were taken as

**Table 1.** Refined structure parameters of  $\text{LiNi}_{0.8}\text{Co}_{0.19}\text{Cu}_{0.01}\text{O}_2$  (powder) in space group  $R\bar{3}m$  at room temperature<sup>a</sup>

Atom	Site	<i>x</i>	<i>y</i>	<i>z</i>	$10^2 \times B$ /nm <sup>2</sup>	Site occupancy
Li1	3a	0	0	0	1.60(3)	0.956
Ni1	3a	=Li1( <i>x</i> )	=Li1( <i>y</i> )	=Li1( <i>z</i> )	=Li1( <i>B</i> )	0.0440(8)
Ni2	3b	0	0	1/2	0.149(6)	0.7741(8)
Li2	3b	=Ni2( <i>x</i> )	=Ni2( <i>y</i> )	=Ni2( <i>z</i> )	=Ni2( <i>B</i> )	0.0278
Co	3b	=Ni2( <i>x</i> )	=Ni2( <i>y</i> )	=Ni2( <i>z</i> )	=Ni2( <i>B</i> )	0.1881
Cu	3b	=Ni2( <i>x</i> )	=Ni2( <i>y</i> )	=Ni2( <i>z</i> )	=Ni2( <i>B</i> )	0.0100
O	6c	0	0	0.24116(2)	0.708(8)	1

<sup>a</sup>Mole fraction:  $\text{LiNi}_{0.8}\text{Co}_{0.19}\text{Cu}_{0.01}\text{O}_2:\text{Li}_2\text{CO}_3 = 0.9831(4):0.0169(4)$ . *B* is an isotropic thermal parameter. Numbers in parentheses are estimated standard deviations of the last significant digits, and parameters without deviations are fixed. *R*-factors are  $R_{\text{wp}} = 8.10\%$ ,  $R_{\text{p}} = 6.00\%$ ,  $R_{\text{exp}} = 3.14\%$ ,  $a = 0.2874210(7)$  nm,  $c = 1.419003(7)$  nm.



**Figure 2.** Rietveld refinement pattern of  $\text{LiNi}_{0.8}\text{Co}_{0.19}\text{Cu}_{0.01}\text{O}_2$  (before charging, Raw). The vertical marks indicate positions of allowed Bragg reflections. The curve at the bottom is the difference between the observed and calculated intensities on the same scale.

**Table 2.** Refined structure parameters of  $\text{LiNi}_{0.8}\text{Co}_{0.19}\text{Cu}_{0.01}\text{O}_2$  (before charge, Raw) in space group  $R\bar{3}m$  at room temperature<sup>a</sup>

Atom	Site	<i>x</i>	<i>y</i>	<i>z</i>	$10^2 \times B$ /nm <sup>2</sup>	Site occupancy
Li1	3a	0	0	0	1.6(5)	0.959
Ni1	3a	=Li1( <i>x</i> )	=Li1( <i>y</i> )	=Li1( <i>z</i> )	=Li1( <i>B</i> )	0.041(5)
Ni2	3b	0	0	1/2	0.19(9)	0.779(5)
Li2	3b	=Ni2( <i>x</i> )	=Ni2( <i>y</i> )	=Ni2( <i>z</i> )	=Ni2( <i>B</i> )	0.022
Co	3b	=Ni2( <i>x</i> )	=Ni2( <i>y</i> )	=Ni2( <i>z</i> )	=Ni2( <i>B</i> )	0.189
Cu	3b	=Ni2( <i>x</i> )	=Ni2( <i>y</i> )	=Ni2( <i>z</i> )	=Ni2( <i>B</i> )	0.01
O	6c	0	0	0.2423(1)	0.58(5)	1

<sup>a</sup>Mole fraction:  $\text{LiNi}_{0.8}\text{Co}_{0.19}\text{Cu}_{0.01}\text{O}_2:\text{Li}_2\text{CO}_3:\text{V} = 0.897(6):0.018(6):0.085(6)$ . *R* factors are  $R_{\text{wp}} = 5.18\%$ ,  $R_{\text{p}} = 3.51\%$ ,  $R_{\text{exp}} = 2.44\%$ ,  $a = 0.287559(3)$  nm,  $c = 1.41918(4)$  nm.

the second and third phases, respectively. These results show close agreement between the cathode and the powder, despite the cathode active material content being approximately 1/100 that of the powder. This demonstrates that it is possible to evaluate the 8.5 mg of active material in the cathode (containing the binder) by neutron diffraction.

Figure 3 shows the profile fitting results for the cathode after charging, and Table 3 shows its crystal structure parameters. The collector aluminum and the vessel V were taken as the second and third phases, respectively. The peaks in the vicinity of  $d = 0.214$  nm are attributable to V and those in the range

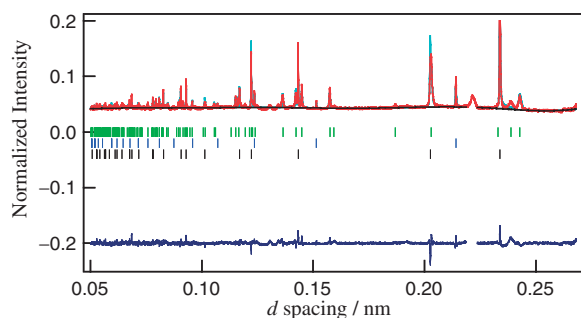


**Figure 3.** Rietveld refinement pattern of  $\text{LiNi}_{0.8}\text{Co}_{0.19}\text{Cu}_{0.01}\text{O}_2$  (after charge, Raw).

**Table 3.** Refined structure parameters of  $\text{LiNi}_{0.8}\text{Co}_{0.19}\text{Cu}_{0.01}\text{O}_2$  (after charge, Raw) in space group  $R\bar{3}m$  at room temperature<sup>a</sup>

Atom Site	<i>x</i>	<i>y</i>	<i>z</i>	$10^2 \times B$ /nm <sup>2</sup>	Site occupancy	
Li1	3a	0	0	0	1.6	0.57(2)
Ni1	3a	=Li1( <i>x</i> )	=Li1( <i>y</i> )	=Li1( <i>z</i> )	=Li1( <i>B</i> )	0.040(3)
Ni2	3b	0	0	1/2	0.19	0.764(3)
Li2	3b	=Ni2( <i>x</i> )	=Ni2( <i>y</i> )	=Ni2( <i>z</i> )	=Ni2( <i>B</i> )	0.04(2)
Co	3b	=Ni2( <i>x</i> )	=Ni2( <i>y</i> )	=Ni2( <i>z</i> )	=Ni2( <i>B</i> )	0.183
Cu	3b	=Ni2( <i>x</i> )	=Ni2( <i>y</i> )	=Ni2( <i>z</i> )	=Ni2( <i>B</i> )	0.012
O	6c	0	0	0.23709(9)	0.7	1

<sup>a</sup>Mole fraction:  $\text{LiNi}_{0.8}\text{Co}_{0.19}\text{Cu}_{0.01}\text{O}_2:\text{V}:\text{Al} = 0.021(2):0.794(2):0.185(2)$ . *R* factors are  $R_{\text{wp}} = 4.39\%$ ,  $R_{\text{p}} = 3.11\%$ ,  $R_{\text{exp}} = 1.73\%$ ,  $a = 0.284491(2)$  nm,  $c = 1.43309(2)$  nm.

**Table 4.** Lattice parameter, cation mixing, BVS,  $\lambda$ ,  $\sigma^2$  of TM (transition metal)–O<sub>6</sub> octahedron for  $\text{LiNi}_{0.8}\text{Co}_{0.19}\text{Cu}_{0.01}\text{O}_2$

Sample	Data	Lattice parameter		Cation mixing		TM–O <sub>6</sub> octahedron			Li <sub>2</sub> CO <sub>3</sub> amount /%
		<i>a</i> /nm	<i>c</i> /nm	Ni at Li site	Li at TM site	BVS	$\lambda$	$\sigma^2$ /deg <sup>2</sup>	
LNCC powder	Raw	0.2874210(7)	1.419003(7)	0.0440(8)	0.0278	2.597	1.005	16.11	1.69(4)
LNCC + AB	Raw-BKG	0.28754(4)	1.4189(5)	0.04(1)	0.02	3.148	1.004	14.17	2.0(9)
+ PVdF, Before	Raw	0.287559(3)	1.41918(4)	0.041(5)	0.022	3.149	1.004	14.17	2.0(6)
LNCC + AB	Raw-BKG	0.284481(5)	1.43306(5)	0.035(7)	0.04(7)	3.379	1.009	29.57	0
+ PVdF, After	Raw	0.284491(2)	1.43309(2)	0.040(3)	0.04(2)	3.415	1.011	36.21	0

$d = 0.2186\text{--}0.2236$  nm to the test instrument; they were, therefore, excluded from the analysis. However, little difference was found between the raw data with the background (instrument and V peaks) excluded (“Raw-BKG”) and the raw data when they were not excluded (“Raw”), indicating that analysis can be effectively performed with either data set. The calculated Li content of the active material is in fair agreement with the analytical Li content by ICP. In summary, the results demonstrate for the first time that it is possible to use neutron diffraction to quantitatively determine the lithium content of the active material and the amount of Li/Ni cation mixing in a coin cell cathode containing a binder and conductive materials after charging.

Table 4 is based on these findings and shows the analytical results in terms of the bond valence sum (BVS) of M(Ni, Co, Cu, Li) located at site 3b and the distortion  $\lambda \cdot \sigma^2$  of the M–O<sub>6</sub> octahedron in each of the three test materials, as obtained from both the raw measurement data (unadjusted) and the raw-BKG measurement data (with instrument and V peaks excluded), and their close agreement. As shown, cathode charging reduced lattice parameter *a* and increased lattice parameter *c*. The contraction in the *a* axis direction is attributable to Li separation and the elongation in the *c* axis direction to increased repulsion between oxygen ions. The results also indicate that the second phase Li<sub>2</sub>CO<sub>3</sub> eliminated by charging and that the difference in cation mixing amount in the cathode before and after charging is not large, indicating that little or none of the mixed Li separates during charge–discharge. In the electrode after charging, the BVS of the M–O<sub>6</sub> octahedron was higher, which is presumably attributable to an increase in the valence of the Ni accompanying Li separation. The increases in  $\lambda$  and  $\sigma^2$  of the M–O<sub>6</sub> octahedron after charging clearly show that M–O<sub>6</sub> octahedral distortion in the cathode is increased by charging.

We used neutron diffraction with Rietveld refinement to analyze solid-state synthesized  $\text{LiNi}_{0.8}\text{Co}_{0.19}\text{Cu}_{0.01}\text{O}_2$  in powder

form and in the cathode of a test coin cell before and after charging. The analysis revealed close agreement between the structural parameters of the powder and those of the ex situ cathode prior to charging, which included an active material together with a binder and a conductor. The results demonstrate for the first time the possibility of neutron-based structural analysis of 8.5 mg of active material in the electrode after charging. The results also reveal that it is possible to quantitatively determine the Li composition, Li/Ni cation mixing, M(Ni, Co, Cu, Li)–O<sub>6</sub> octahedral distortion, and small-quantity second phase component. They also clearly show that, in the active-material system synthesized in this study, the mixed Li does not separate during charge–discharge cycling and that the second phase Li<sub>2</sub>CO<sub>3</sub> is eliminated by charging.

In summary, the results of this study demonstrate that it is possible to perform ex situ structural analysis by neutron diffraction of only 8.5 mg of an active material in a cathode together with the cathode fabrication materials. They also indicate that it will also be possible to perform crystal structure analysis of such cathodes during charge–discharge by in situ neutron diffraction.

#### References

- 1 S.-S. Shin, Y.-K. Sun, K. Amine, *J. Power Sources* **2002**, *112*, 634.
- 2 D. Caurant, N. Baffier, B. Garcia, J. P. Pereira, *Solid State Ionics* **1996**, *91*, 45.
- 3 Y. Idemoto, T. Matsui, *Solid State Ionics* **2008**, *179*, 625; Y. Idemoto, K. Ueki, N. Kitamura, *Electrochemistry* **2010**, *78*, 475.
- 4 R. Oishi, M. Yonemura, Y. Nishimaki, S. Torii, A. Hoshikawa, T. Ishigaki, T. Morishima, K. Mori, T. Kamiyama, *Nucl. Instrum. Methods Phys. Res., Sect. A* **2009**, *600*, 94.
- 5 C. Delmas, I. Saadoun, A. Rougier, *J. Power Sources* **1993**, *43*, 595.
- 6 Z. Wang, Y. Sun, L. Chen, X. Huang, *J. Electrochem. Soc.* **2004**, *151*, A914.
- 7 K. Robinson, G. V. Gibbs, P. H. Ribbe, *Science* **1971**, *172*, 567.